JOURNAL ON COMMUNICATIONS

ISSN:1000-436X

Scopus®

REGISTERED

www.jocs.review

Photocatalytic and Antibacterial Study of Zinc Oxide/Biochar Nanocomposite in Visible Region: Synthesis and Characterisation

Rajesh K M[1*], Devanandha M B[1], Hena C H[1], Laxmi Priya S[1], Manoj N[2], Sreelakshmi K[1]

[1]*Post Graduate and Research Department of Chemistry, Sree Narayana College, Nattika, Thrissur, Kerala – 680566, India, Affiliated to University of Calicut*

2 Post Graduate and Research Department of Chemistry, Sanatana Dharma College, Sanatanapuram, Alapphuzha-688003, India.

Abstract

Water contamination by pathogenic microorganisms and the increasing problem of antimicrobial resistance (AMR) pose serious threats to public health and environmental sustainability, highlighting the need for efficient visible-light-driven antibacterial materials. In this study, a Zinc Oxide/Biochar (ZnO/BC) nanocomposite was synthesized, where biochar derived from onion peel waste through pyrolysis served as a support for ZnO nanoparticles prepared by the sol–gel method. The materials were characterized using X-ray diffraction (XRD), UV–Visible diffuse reflectance spectroscopy (UV–Vis DRS), and Fourier transform infrared spectroscopy (FTIR), confirming the formation of crystalline ZnO with a hexagonal wurtzite structure and its dispersion over the porous biochar surface. Band gap analysis showed a reduction in band gap energy for the ZnO/BC nanocomposite compared to pure ZnO, indicating improved visible-light absorption. Photocatalytic studies under sunlight using crystal violet dye revealed that the ZnO/BC nanocomposite exhibited higher photocatalytic efficiency than pure ZnO due to improved charge separation and enhanced generation of reactive oxygen species (ROS). However, no antibacterial activity against E. coli *was observed under normal conditions. These findings suggest that the ZnO/Biochar nanocomposite is a promising eco-friendly material for visible-light-driven photocatalytic applications in water purification and environmental remediation.*

Keywords: Zinc oxide, Biochar, Nanocomposite, Photocatalytic, Antibacterial, Sun Light, Water purification

1. Introduction

Conventional water disinfection methods, including chlorination, ozonation, and membrane filtration, remain the industry standard; however, these techniques are increasingly scrutinized for their inherent drawbacks. Chlorination is known to produce carcinogenic disinfection by-products, while ozonation and membrane technologies often involve high operational costs and high energy consumption. Consequently, there is an urgent global demand for "next-generation" technologies that are not only cost-effective and efficient but also minimize secondary environmental pollution (1-4).

In recent years, advanced oxidation processes (AOPs) have emerged as effective and environmentally friendly alternatives for modern water treatment. Among these, semiconductor-based photocatalysis has attracted considerable attention due to its unique ability to utilize light energy to drive chemical transformations. This process relies on the generation of high-energy reactive oxygen species (ROS), including hydroxyl radicals (•OH), superoxide radicals (•O_2)and hydrogen peroxide (H_2O_2). These reactive species act as potent oxidants that can effectively degrade organic molecules and inactivate bacteria by causing irreversible damage to their cell membranes, proteins, and nucleic acids, ultimately leading to microbial cell death (5-8).

Zinc oxide (ZnO) stands out as a premier candidate for these applications. As an n-type semiconductor with a wide band gap of approximately 3.2 to 3.37 eV and high exciton binding energy, ZnO is favored for its chemical stability, low toxicity, affordability, and strong oxidative potential. Despite these advantages, pure ZnO exhibits a major limitation: it is primarily active only under ultraviolet (UV) light. Because UV light constitutes only a small fraction of the solar spectrum, and because photogenerated electron–hole pairs in ZnO tend to recombine rapidly, its efficiency under natural visible light remains restricted (9-13).

To overcome these scientific bottlenecks, the formation of composites with carbon-based materials has been widely explored. Biochar, a carbon-rich material obtained through the pyrolysis of organic biomass, possesses a high surface area, a complex porous structure, and excellent electrical conductivity. These physical properties enhance the dispersion of semiconductor nanoparticles, preventing them from clumping together. More importantly, the carbon matrix acts as an electron sink, promoting efficient charge separation and significantly reducing the rate of electron–hole recombination, which allows more ROS to be produced over a longer period. Additionally, biochar is renewable, environmentally friendly, and cost-effective (14-19).

In the present study, onion peels—an abundant and biodegradable agricultural waste—were utilized as the precursor to prepare biochar. This approach directly promotes waste valorization and the development of sustainable materials by turning a zero-value byproduct into a functional tool for environmental remediation. The incorporation of ZnO nanoparticles onto this onion-peel-derived biochar results in a ZnO/Biochar nanocomposite specifically designed to enhance visible light absorption and improve interfacial charge transfer.

Therefore, this work focuses on the systematic synthesis, characterization, and evaluation of the ZnO/Biochar nanocomposite for both antibacterial and visible-light-driven photocatalytic activity. By bridging the gap between agricultural waste management and nanotechnology, the study aims to develop an eco-friendly and highly efficient nanomaterial for potential real-world applications in water disinfection and global environmental protection.

2. Experimental section

2.1 Materials

Zinc chloride ($ZnCl_2$), Sodium hydroxide (NaOH), Isopropyl alcohol (IPA), Crystal violet (CV) was used as received without further purification. Fresh onion peels were collected locally, washed thoroughly with distilled water, and dried before use.

2.2 Preparation of Biochar from Onion Peels

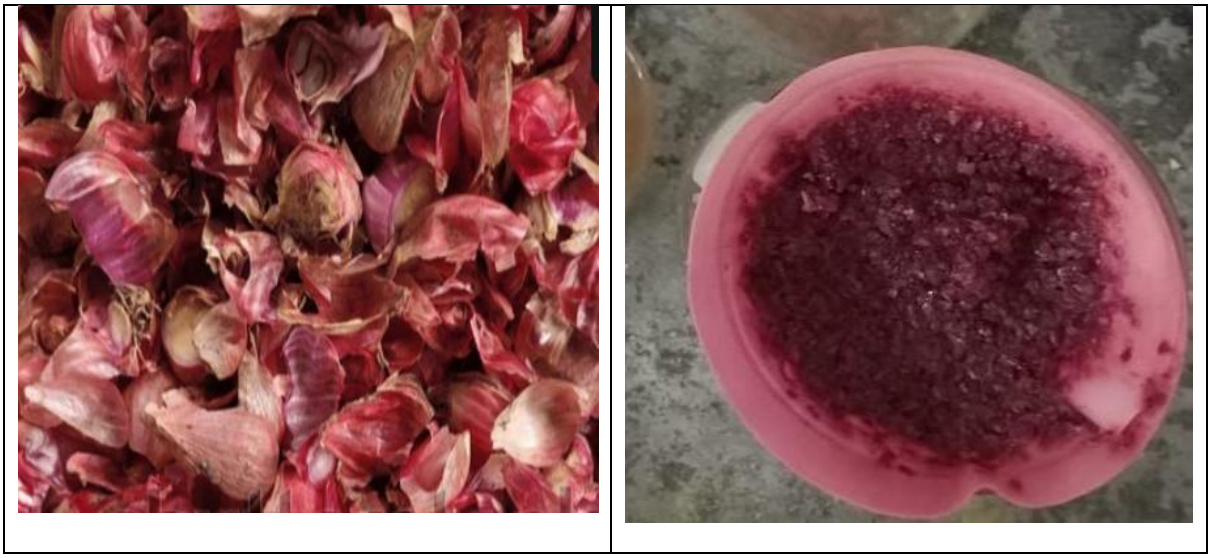

Figure 1. Fresh Onion peel and its processed state

Collected onion peels were grinded and washed with distilled water to remove dust and impurities (figure 1) and then dried in a hot air oven at 60–80°C for 4 hours. The dried peels were subjected to thermal treatment in a muffle furnace at elevated temperature of 300°C for 4 hours to obtain biochar. The resulting biochar was ground into fine powder and stored in airtight containers for further use.

2.3 Synthesis of Catalyst

2.3.1. Synthesis of ZnO/Biochar Nanocomposite (Labelled as ZO)

Prepare 100 ml 0.1M of $ZnCl_2$ in distilled water. To this add, 1 g of onion peel powder was dispersed in 50 mL isopropyl alcohol (IPA) and stirred to obtain a uniform suspension. 10 ml of 5M NaOH solution was added dropwise into the above solution. The mixture was stirred for 60 minutes to ensure complete reaction. The precipitate obtained was dried in a hot air oven 60–80°C for 2 hours. The dried sample was calcined in a muffle furnace 400°C for 3 hours to obtain crystalline ZnO powder.

2.3.2. Synthesis of Pure ZnO (labelled as Zn)

Repeat the above procedure without addition of onion peel powder.

2.4. Preparation of crystal violet solution

0..408g of is crystal violet accurately weighed and dissolved in 1 litter distilled water to make 10^{-3} M solution. From this take 100 ml solution, dilute to 1000ml to make 10^{-4}M solution. Similarly, 10^{-5}M solution is made from 10^{-4} solution.

2.5. Characterisation

The X-ray diffraction (XRD) patterns were recorded using *Bruker* AXS D8 advance X ray Diffractometer with Ni filtered Cu Kα radiation (λ = 0.15406 nm). The intensities were obtained in the 2θ range 10 - 70 ^{0}. The crystallite size was determined from the broadening of the major peak in the XRD spectrum using the Scherrer equation. $D= K \lambda / \beta \cos\theta$. Where D is the crystallite size, K = 0.9 is a constant, λ is the X-ray wavelength, β is full width half maximum of the major peak and θ is the diffraction angle. The UV-Visible diffuse reflectance spectra (UV-Vis.DRS) were recorded in the range of 200-900 nm on a *Labomed* UVD–500 UV-Visible Double beam spectrophotometer equipped with an integrating sphere assembly, using $BaSO_4$ as reflectance standard.The infrared induced vibrations of the samples were recorded using JASCO FTIR spectrometer by means of KBr pellet procedure. Spectra were taken in the transmission mode and the samples were evacuated before making the pellet and the spectra were taken under atmospheric pressure and temperature 293 K.Changes in the absorption bands were investigated in the 400-4000 cm-1 region.

2.6 Photocatalytic Activity Study

Crystal violet photodegradation was used to assess the catalyst's photocatalytic activity. The experiment is carried out in direct sunshine for an average of one hour. A 100 ml beaker was filled with around 10 ml of a 10-5 M crystal violet solution. Add varying amounts of catalyst (0.5 g/L to 1.5 g/L) to this. The adsorption-desorption equilibrium between the catalytic surface and the dye was established by magnetically stirring the system for fifteen minutes in the dark prior to irradiation. The mixture was centrifuged following irradiation. A UV-Visible spectrophotometer set at 590 nm was used to measure the centrifugate's absorbance. The relationship {Co – C} X 100 / Co., where Co and C are the dye concentrations before and after, was then used to determine the percentage of degradation. radiation

2.7Antimicrobial activity by well diffusion method:

The well diffusion method was used to assess the produced catalyst's antibacterial efficacy against Escherichia coli. Mueller-Hinton broth was used to cultivate pure cultures of the organism at 350C and 200 rpm on a rotary shaker. E-coli was uniformly distributed across the surface of Mueller-Hinton agar (MHA) plates. The nanoparticle sample was pipetted into wells that were punched into the agar and had a diameter of 7 mm. As a positive control, ciprofloxacin was employed. After the plates were incubated for a full day, the antibacterial activity was evaluated by measuring the zone of inhibition.

3. Result and Discussion

3.1 Catalyst Preparation

The physical appearance such as colour of the pure zinc oxide (Zn) is white, whereas zinc oxide modified with onion peel powder (ZO) is brownish, but after calcined it gives light brownish white as shown in figure 2. The colour change in modified catalyst compare with pure zinc oxide indicates that the presence of some impurities incorporated into the network of zinc oxide. Later it was confirmed from other characterisation techniques that carbonas matter are these impurities.

(a)

(b)

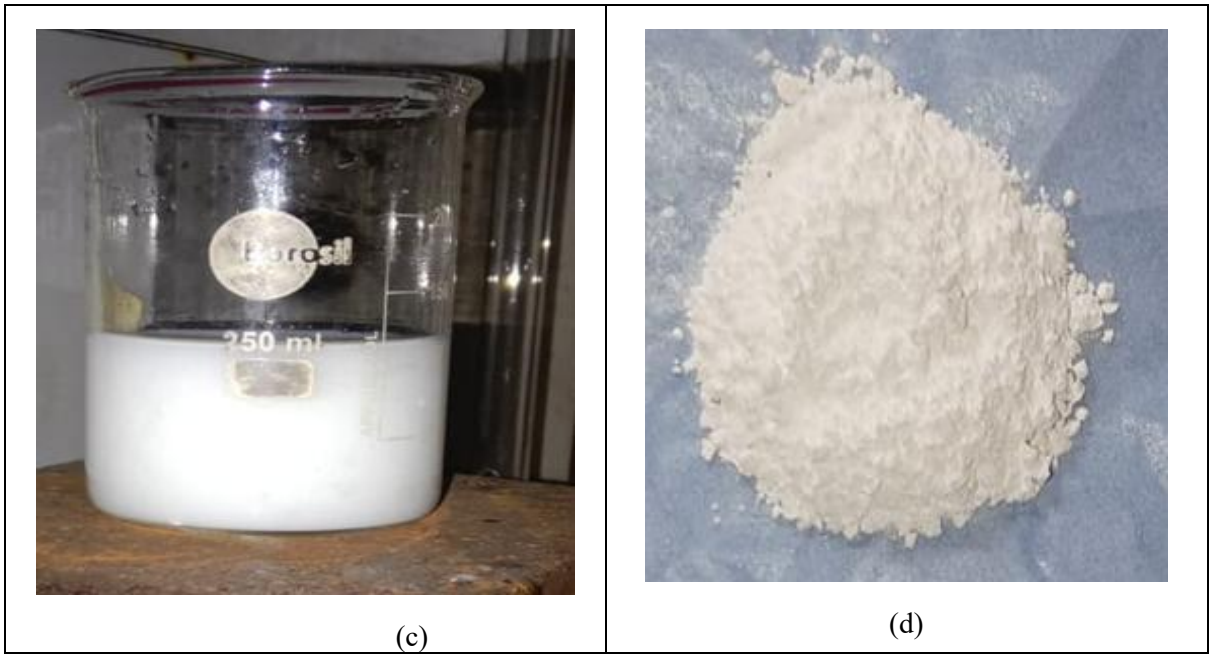

(c) (d)

Figure 2: Onion peel modified ZnO (a) during the preparation, (b) calcined catalyst and pure zinc oxide (c) during the preparation and (d) calcined catalyst.

3.2 FTIR Analysis

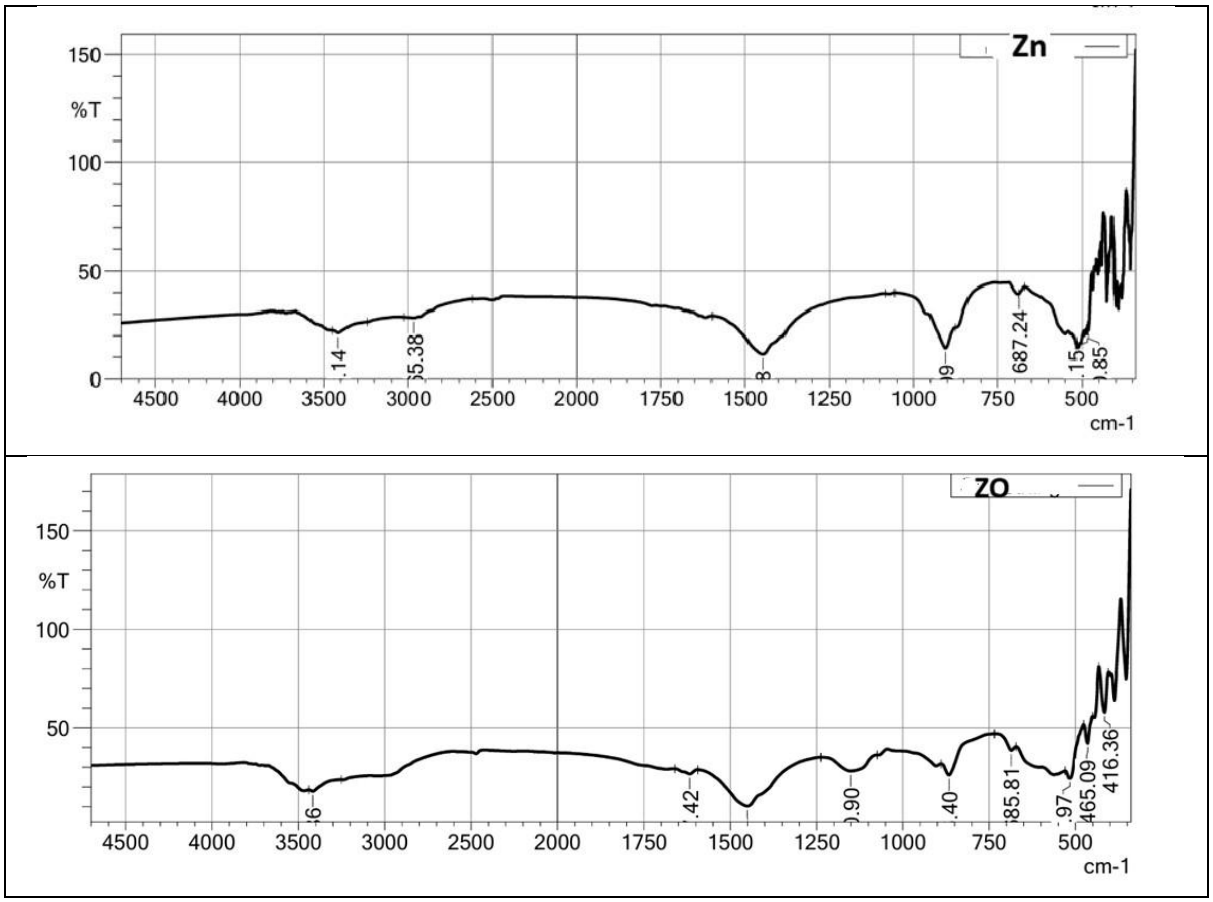

Figure 3. FTIR spectrum of ZO and Zn

The FTIR spectrum of the samples are shown in figure 3. The Fourier Transform Infrared (FTIR) spectra of the synthesized zinc oxide (Zn) and ZO (onion peel modified ZnO), provide critical insights into the formation of the metal oxide framework and the influence of the biological template. In the pure Zn sample, characteristic absorption bands are observed at 408,485 and 687 cm^{-1} . The peaks in the 400-600 cm^{-1} range are attributed to the stoichiometric Zn-O stretching vibrations, confirming the successful synthesis of the wurtzite zinc oxide structure (20). Interestingly, in the ZO sample, these lattice vibrations shift slightly to 416 and 465 cm^{-1}. This shift in the metal-oxygen stretching frequency suggests a modification in the bond lengths or crystalline environment, likely due to the interaction between the ZnO nuclei and the functional groups from the onion peel during the sol-gel process (21).

Both samples exhibit broad absorption features in the higher frequency regions, specifically around 3416 cm^{-1} which are assigned to the O-H stretching vibrations of surface-adsorbed water molecules and structural hydroxyl groups. The presence of these groups is vital for photocatalytic activity as they facilitate the generation of reactive oxygen species. In the Zn sample, a peak at 1447 is observed, while the ZO sample shows a similar band at 1450 along with new peaks at 1617 and 1642. The bands around 1600 – 1640 are characteristic of the bending modes of adsorbed water H-O\-H and C=O or C=C aromatic vibrations derived from the onion peel. The persistence of these peaks in the ZO sample indicates that the biological molecules have effectively modified the surface chemistry, potentially providing more active sites for pollutant adsorption (22,23).

The most significant differences between the two spectra are the additional vibrational modes in the ZO sample, notably at 1150 and 866, and the disappearance of the 2965 peak C-H stretching seen in the pure Zn sample. The band at 1150 is likely associated with the C-O stretching vibrations of polyphenols present in the onion peel. The integration of these organic moieties or their carbonized residues into the ZnO matrix is the primary driver for the narrowing of the band gap. These biomass-derived carbon states introduce intermediate energy levels that allow for visible light excitation, which is consistent with the goal of enhancing photocatalytic efficiency under solar radiation. The shift in the lattice peaks combined with the emergence of these bio-organic signatures confirms the formation of a ZnO/Carbon hybrid material that is chemically distinct from the pure oxide (24).

3.3 X-ray Diffraction

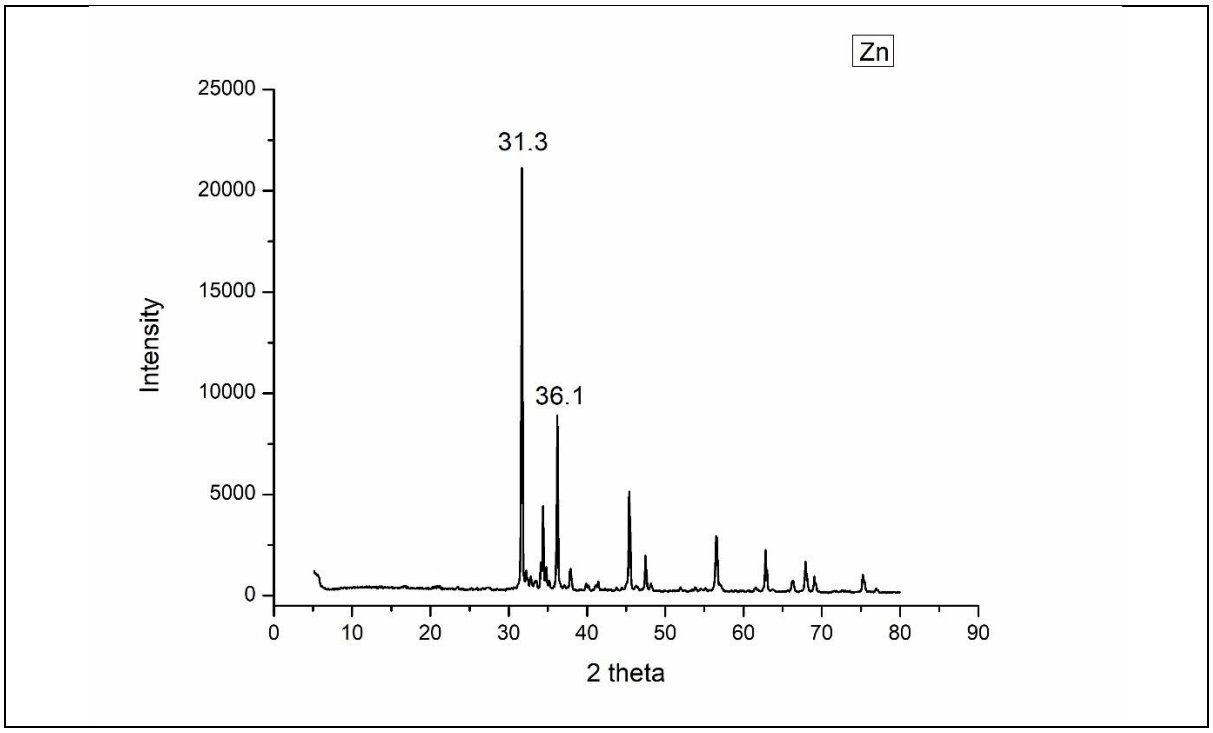

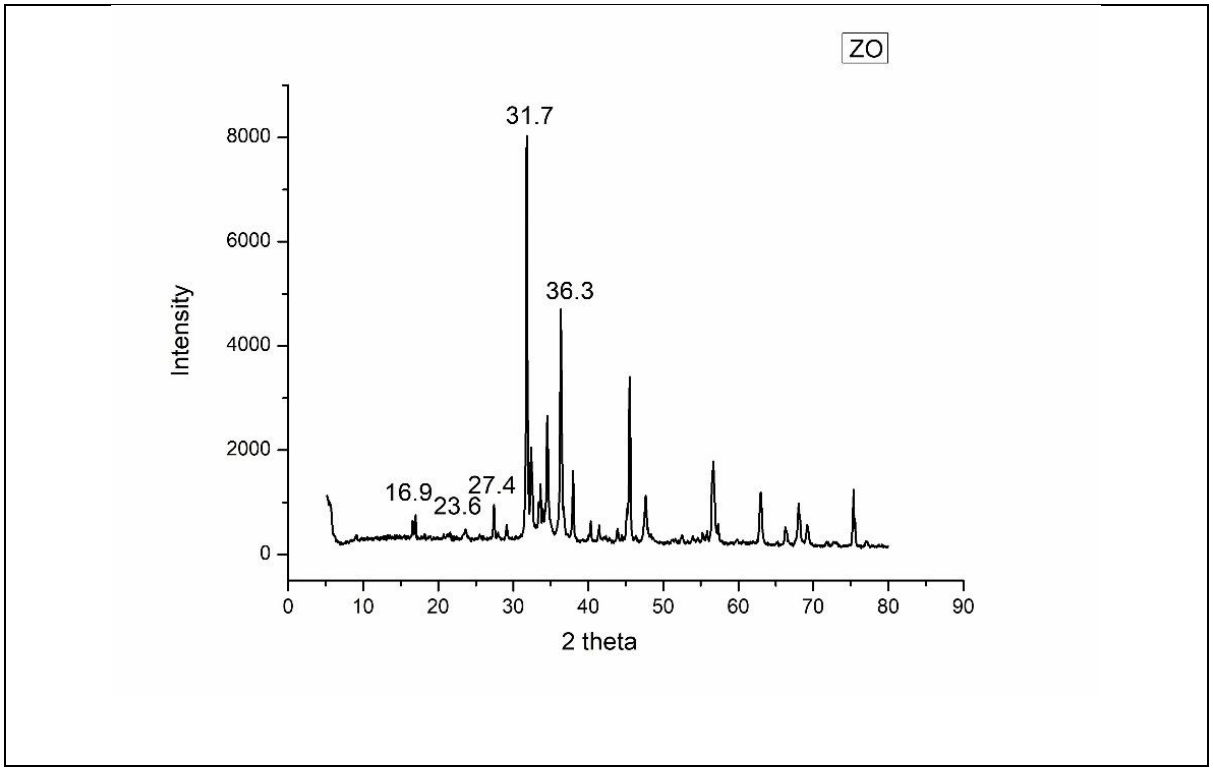

Figure 4: XRD spectrum of Zn and ZO

The XRD spectrum of ZO and Zn are shown in figure 4. Both patterns exhibit sharp, well-defined diffraction peaks at 2theta values of approximately 31.7, 34.4, and 36.2, corresponding to the (100), (002), and (101) planes, respectively. These reflections are characteristic of the hexagonal wurtzite structure of ZnO (JCPDS card no. 36-1451), confirming that the primary crystal lattice remains intact despite the introduction of the biological template. The high intensity of the peaks in both samples indicates a high degree of crystallinity, though the modified ZO sample shows a distinct evolution in peak morphology compared to the pure Zn sample (25).

A significant observation in the XRD data is the broadening of the diffraction peaks in the ZO sample compared to the Zn sample. This broadening is quantitatively analyzed using the Scherrer equation, which relates the peak width to the crystallite size $D = K \lambda / \beta \cos\theta$. The modified sample (ZO) showed a smaller size of 29.5 nm, while the calculated crystallite size for the pure ZnO (Zn) was 44.2 nm. This reduction in crystallite size implies that quercetin and other polyphenols found in the dried onion peel serve as organic "capping agents" during the sol-gel process. A steric barrier that restricts grain growth and stops agglomeration is probably created when these biomolecules adsorb onto the surface of the developing ZnO nucleus. This effect is in line with green synthesis techniques that use plant extracts to regulate the size and shape of nanoparticles (26).

Additional low-intensity peaks with 2theta values of 16.9, 23.6, and 27.4 are visible in the ZO sample's XRD pattern. The remaining carbonaceous materials or mineral complexes formed from the onion peel template are responsible for these peaks, which are not present in the pure Zn pattern. The organic matter partially carbonizes during the thermal treatment, which may result in the integration of carbon species into the lattice or the creation of a ZnO/Carbon composite. The desired band gap decrease depends on this integration. These bio-derived components increase the material's photocatalytic potential and enable visible light absorption by generating new electronic states between the valence and conduction bands (20).

The structural modifications observed in the ZO sample—specifically the reduced crystallite size and the presence of bio-residue peaks—provide a clear pathway for improved optical properties. The

reduction in size to 29.5 nm significantly increases the surface-to-volume ratio, providing more active sites for surface reactions. Furthermore, the interaction between the ZnO precursors and the onion peel functional groups facilitates a "self-doping" mechanism where carbonaceous species sensitize the semiconductor. This synergy effectively explains the shift in the absorption edge toward the visible region, making the onion peel-mediated ZnO a more efficient material for environmental remediation than its pure counterpart produced via the standard sol-gel route.

3.4 UV-Visible diffuse reflectance spectra

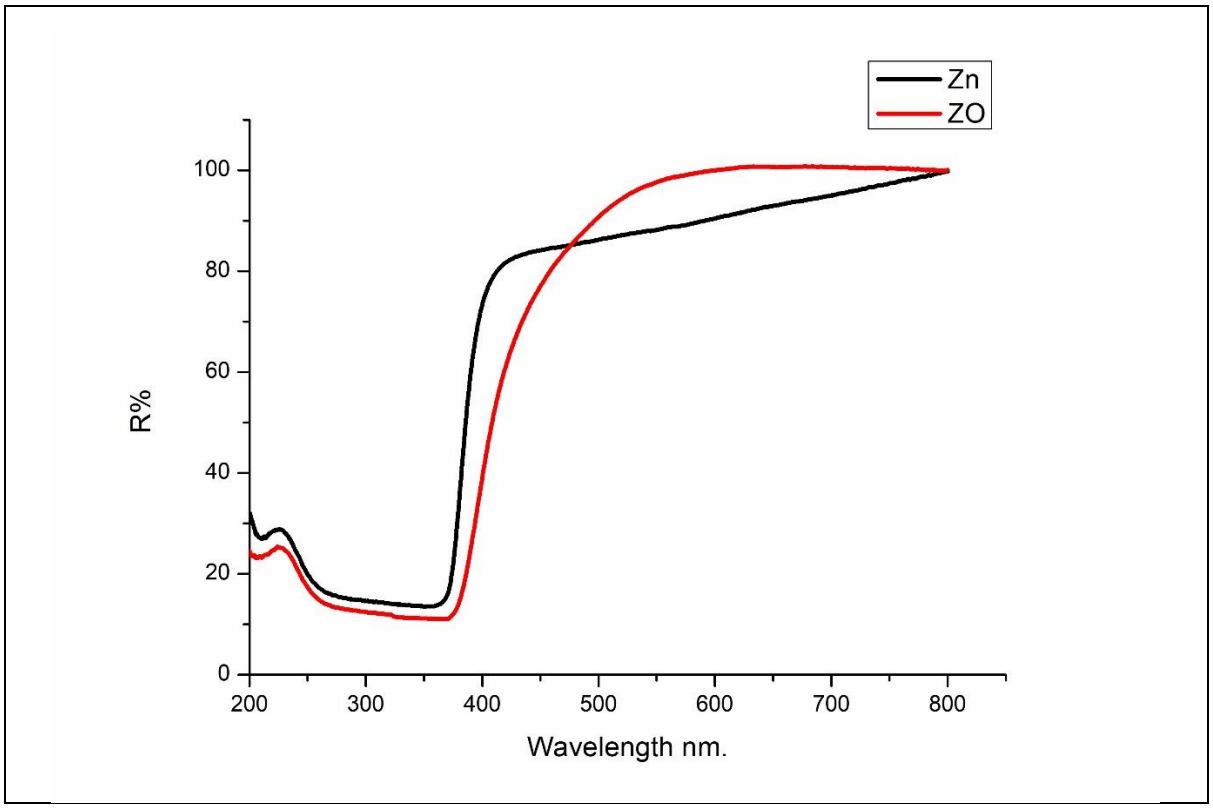

Figure. 5 UV-Visible DRS of ZO and Zn

UV-visible diffuse reflectance spectroscopy (DRS) was used to assess the optical characteristics and light-harvesting capacity of the produced zinc oxide samples, as illustrated in figure 5. The absorption edge lambda was found from the abrupt drop in reflectance in the ultraviolet-visible range in order to calculate the optical band gap Eg. In contrast to the onion peel-modified sample (ZO), which has an absorption edge that extends to around 505 nm, pure ZnO (Zn) displays an absorption edge at about 395 nm.

Applying the link between energy and wavelength, the band gap for pure ZnO (Zn) is determined to be 3.14 eV, which is compatible with the typical electrical structure of wurtzite ZnO. This formula, Eg = Band gap (eV) = 1240 / λ (nm), is one of the simplified versions of KM, Kubelka-Munk, equation. The modified sample (ZO), on the other hand, shows a noticeably reduced band gap of 2.46 eV. The successful conversion of ZnO into a visible-light-active semiconductor by adding dried onion peel is confirmed by this 0.68 eV reduction (27).

For a rigorous quantitative determination suitable for high-impact scientific reporting, the raw reflectance data (R) must be transformed into the Kubelka-Munk absorption function(R). Since ZnO is characterized by a direct electronic transition, a Tauc plot is typically constructed by plotting F(R) against photon energy. The linear extrapolation of these plots to the x-axis provides a precise optical band gap measurement. The observed shift from 3.14 eV to 2.46 eV suggests that the organic functional groups and mineral content from the onion peel introduced new electronic states within the forbidden

zone. This phenomenon is often attributed to the formation of a carbon-ZnO composite or in-situ carbon doping during the thermal treatment of the biomass template

The structural changes shown in the earlier XRD and FTIR investigations are closely linked to the narrowing of the band gap in sample ZO. The biomass functioned as a capping agent, raising the surface-to-volume ratio and the density of active surface states, as evidenced by the XRD reduction in crystallite size from 44.2 nm (Zn) to 29.5 nm (ZO). Additionally, the presence of residues produced from biomass was confirmed by the FTIR data, which showed the formation of peaks at 1150 cm^{-1} and 866 cm^{-1}. By acting as sensitizers, these residues successfully reduce the energy needed for electrical excitation from the valence band to the conduction band. This synergistic effect not only narrows the band gap but also enhances the material's ability to utilize a broader range of the solar spectrum, making the ZO sample a superior candidate for visible-light-driven photocatalytic applications.

3.5 Anti-bacterial study

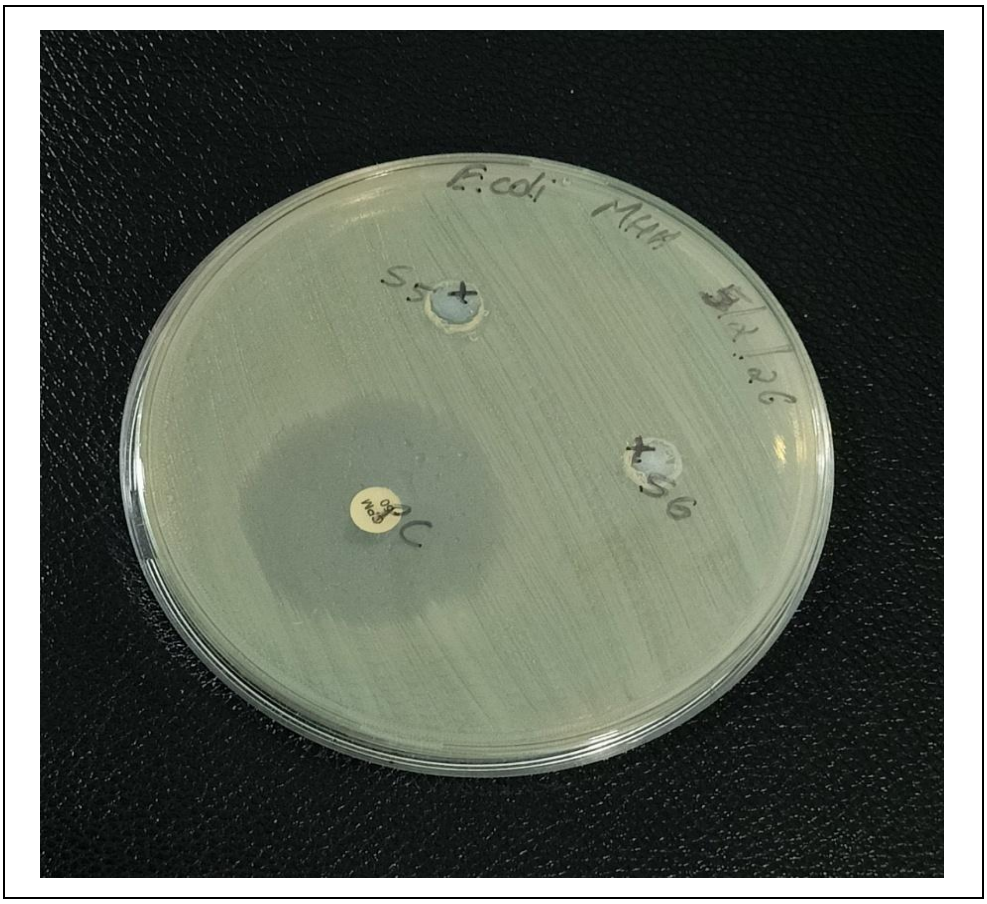

Figure 6: Inhibition zone of E-coli growth for Z(S5), Zn(S6), C control

The antibacterial efficacy of the pure zinc oxide (Zn) and onion peel-modified zinc oxide (ZO) was assessed against *Escherichia coli* using the agar well diffusion method on Mueller-Hinton Agar (MHA). Based on the experimental observations, neither the pure Zn nor the modified ZO produced a measurable zone of inhibition, whereas the positive control (C) exhibited a clear and distinct area of bacterial growth suppression. These results indicate that under the specific dark conditions of this study, *E. coli* remains resistant to the ZnO nanostructures, regardless of the biological modification or the reduced crystallite size of 29.5 nm calculated earlier. The absence of dark toxicity is a common characteristic of high-purity metal oxide semiconductors synthesized via green routes (28,29).

The Zn and ZO catalysts' photocatalytic properties are directly responsible for the observed absence of antibacterial activity. The production of Reactive Oxygen Species (ROS), such as hydroxyl radicals (OH*) and superoxide anions (O2-), is the main way that zinc oxide, a semiconductor, promotes the breakdown of microbial cells. But in order to produce these species, electrons must be excited from the valence band to the conduction band, a process that can only be started by photon absorption. Because there was no light source during this experiment, the catalysts stayed dormant and were unable to create the oxidative stress required to break through the intricate cell wall of Gram-negative E. coli. This confirms that while the onion peel modification successfully narrowed the band gap to **2.46 eV**, the material requires solar or visible light irradiation to exhibit its biocidal potential (30).

The resilience of E. coli in the dark highlights the fact that the changes seen in FTIR and XRD, like the shift in Zn-O lattice peaks and the integration of carbonaceous residues, are tailored for electrical toxicity rather than chemical toxicity. In order to inhibit bacteria in the dark, ZnO nanoparticles typically rely on the release of Zn 2+ ions or direct physical contact; however, these samples' stable wurtzite structure probably reduced ion leakage. The red-shift in the DRS spectra indicates that the structural synergy seen in the ZO sample especially improves its capacity to capture visible light. As a result, these particular catalysts' antibacterial activity should be regarded as "latent," requiring photocatalytic activation to change from a bio-inert to a bio-active state (31).

3.6 Photocatalytic activity

Crystal violet is a heterocyclic aromatic chemical compound with the molecular formula $C_{25}H_{30}ClN_3$. At room temperature it appears as a deep violet or purple powder, which yields a violet solution when dissolved in water and gives characteristic spectrophotometric absorbance at 590 nm.

a. Effect of catalyst amount and dye concentration

A 10^{-5} molar aqueous solution of crystal violet was used in this study. About 10 ml of 10^{-5} M solution was taken and catalyst amount of 0.5g/L to 1.5 g/L was added. Before irradiation the system was magnetically stirred for 15 minutes under dark to establish the adsorption-desorption equilibrium between the catalytic surface and the dye. The absorbance of the solution before and after the irradiation 30 minute with solar light was measured using spectrophotometer at 590 nm.

Table 1: % Degradation of crystal violet against amount of catalyst, Irradiation time: 30 minutes

Catalyst	Amount of catalyst (g/L)	% degradation
ZO	0.005 g	65
	0.01 g	90
	0.015 g	93
Zn	0.005 g	30
	0.01 g	40
	0.015 g	43
Without Catalyst	0.01 g	4

(a) (b) (c)

Figure 7: (a) Crystal violet before light irradiation, (b) after 30-minute irradiation in sunlight using pure Zinc oxide (Zn) and (c) that of onion peel muddied Zinc oxide (ZO).

The percentage of crystal violet degradation against various catalyst dosages is shown in Table 1 and fig 7. The data show that the percentage of degradation rises as the amount of catalyst increases, reaches a maximum, and then becomes independent of catalyst concentration. Therefore, a key factor in photocatalytic dye degradation is the amount of catalyst. An increase in the percentage of degradation could also be caused by an increase in the number of active sites on the catalyst surface for the reaction and an increase in light absorption. As the amount of catalyst increased, more photons were adsorbed, and more dye molecules were adsorbed due to an increase in ZnO particles.

The density of particles in the area of illumination also increases and so the rate is enhanced. Above a certain level, the substrate molecules available are not sufficient or adsorption by the increased number of ZnO particles, i.e. although more area is available, for a constant the number of substrate molecules present in the solution is the same. Hence the additional catalyst powder is not involved in catalyst activity and the rate does not increase with an increase in the amount of catalyst beyond a certain limit

Thus, the optimum catalyst amount in this case is 1 g/L. At higher amount, the vacant sites are consumed by the intermediate products during the reaction which retards the further degradation of the substrate and hence the percentage degradation decreased or retained without a noticeable change. The higher activity is also attributed to the highly ordered nature of the catalyst and its method of preparation which are favourable factors for photocatalytic activity.

b. Effect of time.

Studies involve a 50 ml of 10^{-5} molar aqueous solution of crystal violet with a catalyst amount of 1 g/L, which was optimized by the above experiment. Before irradiation the system was magnetically stirred for 10 minutes under dark to establish the adsorption-desorption equilibrium between the catalytic surface and the dye. After irradiation with sun light, 10ml of the suspension was pipette out from the solution at an interval of 10 minutes. The pipetted sample was filtered and measured the absorbance at 590 nm.

Table 2: % Degradation of crystal violet against time, amount of Catalyst: 1 g/L; Dye con. 10 ml of 10^{-5} M

Time (minutes)	Percent Degradation
10	30
20	65
30	91

40	93
50	96
60	100

The degradation of crystal violet by photocatalysis in relation to irradiation time is displayed. Table 2 The data show that the percentage degradation increases linearly with time. There is no discernible change after this one-hour time restriction (which is not depicted in the figure). The outcome shows that the percentage of degradation rises with increasing irradiation time and peaks at one hour of exposure. However, it was shown that after 30 minutes, almost 90% degradation takes place. As time passes, an increasing amount of light energy strikes the catalyst surfaces, increasing the production of photoexcited species and boosting photocatalytic activity.

4. Conclusion

The sol–gel synthesis using dried onion peel biomass powder successfully produced visible-light-responsive hexagonal wurtzite nanocrystalline ZnO. FTIR analysis confirmed the formation of the ZnO lattice and revealed biomass-derived functional groups in the modified sample (ZO), particularly bands at 1150 and 866 cm^{-1}, indicating the incorporation of onion peel residues containing phenolic and hydroxyl groups. XRD results showed that both pure and modified samples crystallized in the hexagonal wurtzite phase, while the introduction of the biological template reduced the crystallite size from 44.2 nm to 29.5 nm, with additional peaks at 16.9°, 23.6°, and 27.4° suggesting the presence of carbonaceous or mineral components from the onion peel. Optical studies using diffuse reflectance spectroscopy and Tauc plot analysis revealed a reduction in the band gap from 3.14 eV for pure ZnO to 2.46 eV for the modified sample, attributed to reduced crystallite size and biomass-induced surface defects and oxygen vacancies, which enhance visible-light absorption. Photocatalytic studies using 10^{-5} M crystal violet under solar irradiation demonstrated strong activity, achieving more than 90% dye degradation within 30 minutes at a catalyst loading of 1 g L^{-1} due to improved charge separation and visible-light response. However, antibacterial tests against *E. coli* showed no zone of inhibition for both Zn and ZO samples under dark conditions, indicating that the catalysts require light activation to generate reactive oxygen species (ROS) and therefore act as light-dependent antibacterial agents.

5. Acknowledgment:

We are deeply grateful for the support provided by the DBT-STAR and RUSA program of Sree Narayana College, Nattika. We also extend our sincere thanks to Veta Genomics, Thrissur, as well as the Departments of Botany and Zoology at Sree Narayana College for their valuable contributions to the antibacterial studies and data interpretation.

6. References

1. I. Manisalidis, E. Stavropoulou, A. Stavropoulou and E. Bezirtzoglou, “Environmental and health impacts of air pollution: A review”, Front. Public Health, 8, (2020), pp. 1-13.
2. N. J. Ashbolt, “Microbial contamination of drinking water and disease outcomes in developing regions”, Toxicology, 198, (2004), pp. 229-238.
3. M. A. Shannon, P. W. Bohn, M. Elimelech, J. G. Georgiadis, B. J. Marinas and A. M. Mayes, “Science and technology for water purification in the coming decades”, Nature, 452, (2008), pp. 301-310.
4. S. D. Richardson and T. A. Ternes, “Water analysis: Emerging contaminants and current issues”, Anal. Chem., 90, (2018), pp. 398-428.
5. J. M. Poyatos, M. M. Muñio, M. C. Almecija and J. C. Torres, “Advanced oxidation process for waste water treatment: State of the art”, Water Air Soil Pollut., 205, (2010), pp. 187-204.
6. A. Fujishima, X. Zhang and D. A. Tryk, “TiO_2 photocatalysis and related surface phenomenon”, Surf. Sci. Rep., 63, (2008), pp. 515-582.
7. M. N. Chong, B. Jin, C. W. K. Chow and C. Saint, “Recent developments in photocatalytic water treatment technology: A review”, Water Res., 44, (2010), pp. 2997-3027.
8. H. A. Foster, I. B. Ditta, S. Varghese and A. Steele, “Photocatalytic disinfection using titanium dioxide: Spectrum and mechanism of antimicrobial activity”, Appl. Microbiol. Biotechnol., 90, (2011), pp. 1847-1868.

9. U. Özgür, Y. I. Alivov and C. Liu, "A comprehensive review of ZnO materials and device", J. Appl. Phys., 98, (2005), pp. 041301-103.
10. B. Abebe, C. A. Ananda Murthy and E. A. Zereffa, "Enhancing the photocatalytic efficiency of ZnO: Defects, heterojunction and optimization", Environ. Nanotechnol. Monit. Manag., 14, (2020), pp. 100336.
11. T. Iqbal, M. A. Khan and H. Mahmood, "Facile synthesis of ZnO nanosheets: Structural, antibacterial and photocatalytic studies", Mater. Lett., 224, (2018), pp. 59-63.
12. K. R. Raghupati, R. T. Koodali and A. C. Manna, "Size-dependent bacterial growth inhibition and mechanism of antibacterial activity of zinc oxide nanoparticles", Langmuir, 27, (2011), pp. 4020-4028.
13. L. V. Bora and R. K. Mewada, "Visible/solar light active photocatalyst for organic effluent treatment: Fundamentals, mechanism and parametric review", Renew. Sustain. Energy Rev., 76, (2017), pp. 1393-1421.
14. G. Alberta, I. Elisa, L. Garcla, A. Narimene, M. Bartolo, A. C. Conchi and M. Giuseppe, "Carbon based composite materials as photocatalyst for photo-reforming of organics to obtain H_2", Chem. Eng. Trans., 119, (2025), pp. 55-60.
15. L. Leng, X. Yuan, G. Zeng, J. Shao, X. Chen, Z. Wu, H. Wang and X. Peng, "Surface characterisation of rice husk bio-char produced by liquefaction and application for cationic dye (malachite green) adsorption", Fuel, 155, (2015), pp. 77-85.
16. G. Jun, W. Yue, Z. Yanfie, Z. Meiting and T. Zhiyong, "Advanced photocatalyst based on metal nanoparticles/metal-organic framework composites", Nano Res., 14, (2021), pp. 2037-2052.
17. M. Dinesh, S. Ankur, O. Yong S and P. Jr Charles U, "Organic and inorganic contaminants removal from water with biochar, a renewable, low cost and sustainable adsorbent: A critical review", Bioresour. Technol., 160, (2014), pp. 191-202.
18. X. Jun, H. Yubo, Z. Shihui, A. Nedra, J. Xioaning and Z. Liang, "A review of the green synthesis of ZnO nanoparticles using plant extracts and their prospects for application in antibacterial textiles", J. Eng. Fibers Fabr., 16, (2021), pp. 1-14.
19. S. Shubham, O. Sachin and J. Jyoti, "Biochar based photocatalyst for degradation of organic aqueous waste: A review", Chemosphere, 287, (2022), pp. 132200.
20. H. S. Shahraki, Q. Qurtulen and A. Ahamad, "Synthesis and characterization of carbon dots from onion peel and their application as adsorbent and anticancer activity", Inorg. Chem. Commun., 150, (2023), pp. 110514.
21. A. R. Prasad, J. Garvasis, S. Kunnekkat Oruvil and A. Joseph, "Bio-inspired green synthesis of zinc oxide nanoparticles using Abelmoschus esculentus mucilage and selective degradation of cationic dye pollutants", J. Phys. Chem. Solids, 127, (2019), pp. 265-274.
22. B. Thangaraj, N. Wongyao, P. R. Solomon, V. Gupta, A. Abdullah, S. Abedrabbo and J. Hassan, "Synthesis of reduced graphene oxide from onion peel waste by single-stage pyrolysis, characterization and evaluation of its antibacterial activity", J. Environ. Chem. Eng., 12, (2024), pp. 113474.
23. S. Modi, V. K. Yadav, N. Choudhary, A. M. Alswieleh, A. K. Sharma, A. K. Bhardwaj, S. H. Khan, K. K. Yadav, J. K. Cheon and B. H. Jeon, "Onion peel waste mediated-green synthesis of zinc oxide nanoparticles and their phytotoxicity on mung bean and wheat plant growth", Materials, 15, (2022), pp. 2393.
24. W. Kuncoro, A. Sanata, S. Junus, N. Ilminnafik and A. Triono, "The effect of activated carbon onion peel flavonoids on hydrogen production by photocatalyst method", J. Penelit. Pendidik. IPA, 9, (2023), pp. 12276-12282.
25. S. Soltani, A. Gacem, N. Choudhary, V. K. Yadav, H. Alsaeedi, S. Modi, A. Patel, S. H. Khan, M. M. S. Cabral-Pinto, K. K. Yadav and A. Patel, "Scallion peel mediated synthesis of zinc oxide nanoparticles and their applications as nanofertilizer and photocatalyst for removal of organic pollutants from wastewater", Water, 15, (2023), pp. 1672.
26. S. Zeghoud, H. Hemmami, B. Ben Seghir, I. Ben Amor, I. Kouadri, A. Rebiai, M. Messaoudi, S. Ahmed, P. Pohl and J. Simal-Gandara, "A review on biogenic green synthesis of ZnO nanoparticles by plant biomass and their applications", Mater. Today Commun., 33, (2022), pp. 104747.
27. D. Channei, P. Thammaacheep and P. Jannoey, "Utilizing banana peel in conjunction with TiO_2 photocatalyst for the efficient decolorization of malachite green", Chem. Phys. Impact, 8, (2024), pp. 100629.
28. A. R. Mendes, C. M. Granadeiro, A. Leite, O. Geiss, I. Bianchi, J. Ponti, D. Mehn, E. Pereira, P. Teixeira and F. Poças, "Functional properties and safety considerations of zinc oxide nanoparticles under varying conditions", Nanomaterials, 15, (2025), pp. 892.
29. Z. Jowkar, S. Askarzadeh, S. A. Hamidi, Z. Fattah and A. Moaddeli, "Assessment of the antimicrobial properties of mesoporous zinc oxide nanoparticles against Streptococcus mutans: An in vitro investigation", Int. J. Dent., (2025), pp. 1-10.
30. S. Gharpure, R. Yadwade and B. Ankamwar, "Non-antimicrobial and non-anticancer properties of ZnO nanoparticles biosynthesized using different plant parts of Bixa orellana", ACS Omega, 7, (2022), pp. 1914-1933.
31. N. Zubair, R. M. S. Al-Oqaili, M. J. Yousaf, A. Siddique, F. A. Awwad, E. A. A. Ismail, F. Shams, A. Aldhahrani, N. Itrat, F. Ali, D. P. Rao, H. Khalid, F. Ali, F. A. Al-Salmi, M. A. Alenezi, H. I. Thalib and J. H. Timraz, "Morphology dependent antibacterial activity of zinc oxide nanoparticles against clinically relevant bacteria", Sci. Rep., 15, (2025), pp. 45186-18.